Inorganic Chemistry

Article

pubs.acs.org/IC

Thermodynamic N-Donor trans Influence in Labile Pseudo-Octahedral Zinc Complexes: A Delusion?

Lilit Aboshyan-Sorgho,[†,§] Timothée Lathion,[†,§] Laure Guénée,[‡] Céline Besnard,[‡] and Claude Piguet*[,†]

[†]Department of Inorganic and Analytical Chemistry, and [‡]Laboratory of Crystallography, University of Geneva, 30 quai E. Ansermet, CH-1211 Geneva 4, Switzerland

Supporting Information

ABSTRACT: While the forces responsible for the chelate effect are well-established in coordination chemistry, the origin and implementation of the related thermodynamic trans influence remains debatable. This work illustrates a simple approach for quantifying this effect in labile pseudo-octahedral $[Zn(\mathbf{Lk})_3]^{2+}$ complexes lacking stereochemical preferences (**Lk** = **L1**−**L4** are unsymmetrical didentate α,α'-diimine ligands). In line with statistics, the triply degenerated meridional isomers *mer*-$[Zn(\mathbf{Lk})_3]^{2+}$ are stabilized by $0.8 \leq \Delta G_{exch}^{mer\rightarrow fac} \leq 4.2$ kJ/mol over their nondegenerated facial analogues *fac*-$[Zn(\mathbf{Lk})_3]^{2+}$ and therefore display no apparent trans influence at room temperature. However, the dissection of the free energy terms into opposite enthalpic (favoring the facial isomers) and entropic (favoring the meridional isomers) contributions reveals a trans influence assigned to solvation processes occurring in polar solvents. Altogether, the thermodynamic trans influence operating in $[Zn(\alpha,\alpha'\text{-diimine})_3]^{2+}$ complexes is 1−2 orders of magnitude smaller than the chelate effect. A weak templating effect provided by a noncovalent lanthanide tripod is thus large enough to produce the wanted facial isomer at room temperature.

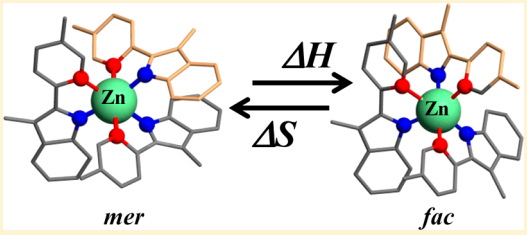

INTRODUCTION

Chelate effects and trans influence are thermodynamic processes representing well-established landmarks for controlling complexation processes in coordination chemistry.[1] A large part of the experimental data supporting these concepts originates from the complexation of multidentate polyaminocarboxylates[2] and of 2,2′-dipyridine (**L0**), the archetype of the α,α'-diimine binding unit,[3] with open-shell d-block cations. For instance **L0**, and a wealth of its derivatives bearing peripheral substituents, were connected to the kinetically inert and photophysically active d^6 low-spin Ru(II) to give six-coordinated complexes that are expected to optimize the light-harvesting process operating in dye-sensitized solar cells.[4] Structurally speaking, the pseudo-octahedral D_3-symmetrical $[Ru(\mathbf{L0})_3]^{2+}$ complex exists as a pair of kinetically inert helical enantiomers (Δ/Λ), which can be separated by crystallization or by chromatography using chiral partners.[5]

Drastic changes may be induced by the replacement of one of the pyridine rings with a different heterocycle (imidazole, pyrazole, diazine, thiophene, etc.) as illustrated in the didentate ligands **L1** and **L2**, in which a benzimidazole ring is connected to a pyridine unit. The remaining pyridine ring itself can be

Scheme 1. Chemical Structures of the Didentate Ligands L0−L4 in Their Relaxed Transoid Conformations

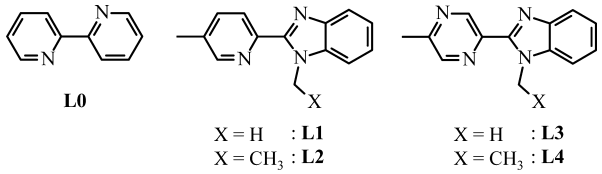

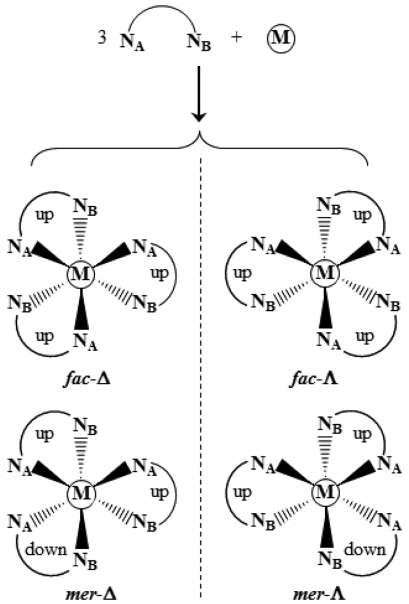

Figure 1. Schematic representation of the two pairs of enantiomers produced by the complexation of three nonsymmetrical didentate ligands about an octahedral metallic center.

Received: September 17, 2014
Published: November 19, 2014

 © 2014 American Chemical Society dx.doi.org/10.1021/ic5022559 | *Inorg. Chem.* 2014, 53, 13093−13104

modified with the introduction of a second heteroatom as found in **L3** and **L4** (Scheme 1).[6] In the nonsymmetrical ligands **L1**−**L4**, the internal 2-fold symmetry axis found in **L0** is removed, and the saturated homoleptic pseudo-octahedral $[M(\mathbf{Lk})_3]^{2+}$ complexes (**Lk** = **L1**−**L4**) exist as facial (fac, C_3 symmetry) and meridional (mer, C_1 symmetry) stereoisomers, each being constituted of a pair of helical Δ/Λ enantiomers (Figure 1).[7]

Simple geometrical considerations show that a single microspecies contributes to the facial isomer (up−up−up, Figure 1), while the meridional isomer is made up of three isoenergetic microspecies (up−up−down/up−down−up/down−up−up, Figure 1).[8] One also notes that, in the facial isomer, each donor atom N_A of a given heterocycle lies trans to the N_B donor atom of another aromatic ring thus leading to three trans N_A−M−N_B correlations. In the meridional isomer, a single heterotopic trans N_A−M−N_B arrangement occurs, together with two trans homotopic N_A−M−N_A and N_B−M−N_B correlations (Figure 1).[9] Since electronic (spin-crossover),[10] photophysical (energy gap, excited-state lifetime, quantum yield),[11] electrochemical,[12] and physical (metalorganic chemical vapor deposition)[13] properties depend on the ligand-field strength and on the exact geometries around the metallic center, the control of the *mer*-$[ML_3]$ ↔ *fac*-$[ML_3]$ isomerization process is crucial for programming and optimizing the physicochemical characteristics of the final complex.[5,14] While the dynamics of the intimate mechanisms of mer↔mer and mer↔fac isomerization processes around various labile closed-shell metallic cations was the focus of comprehensive kinetic studies,[7,15,16] we cannot find reliable thermodynamic analysis of equilibrium (1) for labile octahedral complexes in solution except for the paramagnetic open-shell d^7 complex $[Co(\mathbf{L1})_3]^{2+}$ in acetonitrile.[15]

$$mer\text{-}[ML_3] \rightleftharpoons fac\text{-}[ML_3] \quad K_{mer\rightarrow fac} = \frac{[fac\text{-}ML_3]}{[mer\text{-}ML_3]} \qquad (1)$$

The primary source of pseudothermodynamic analysis of the equilibrium constant $K_{mer\rightarrow fac}$ relies on the integration of the NMR spectra recorded on mixtures produced by the reactions of ruthenium salts with derivatives of **L0**[17] or **L1**[18] under harsh conditions. The final mer/fac ratios systematically deviate from the expected statistical 3/1 distribution,[19] and two empirical rules have been formulated for rationalizing this drift: (1) The meridional isomer is stabilized by the implementation of steric crowding close to one coordinating donor atoms of the nonsymmetrical didentate α,α′-diimine unit (a single unfavorable cis N_A−M−N_A, or cis N_B−M−N_B, correlation operates in the mer isomer, while three such interactions exist in the fac isomer, Figure 1).[17a] (2) The facial isomer is stabilized by the coordination of unsymmetrical push−pull didentate α,α′-diimine binding units,[17b] the latter trend being assigned to the so-called thermodynamic trans influence, which states that the donor atom of the electron-withdrawing heterocyclic ring preferably lies trans to the donor atom of the electron-releasing heterocyclic ring (three favorable trans N_A−M−N_B correlations are implemented in the fac isomer, while only one occurs in the mer analogue, Figure 1).[20] The trans influence seems to be weak since the meridional isomer usually dominates the speciation in solution,[15−18] and the selective preparation of C_3-symmetrical *fac*-$[ML_3]$ complexes thus relies on template syntheses where the unsymmetrical didentate binding units are tethered to covalent[11b,21] or noncovalent[18,22] tripods. However, both cis and trans influences were deduced from changes in bond lengths observed in the crystal structures of octahedral metal complexes,[20,23] and a rational thermodynamic analysis of the formation and isomerization of labile $[M(\mathbf{Lk})_3]^{2+}$ in solution (**Lk** = **L1**−**L4**) could unravel the use of the trans influence for preparing the statistically least-favored facial isomer. We report here on the origin and magnitude of the trans influence induced by the replacement of the pyridine rings in **L1** and **L2** with the electron-rich pyrazine rings in **L3** and **L4**. With its spherical $[Ar]3d^{10}4s^0$ electronic configuration, M = Zn(II) is ideally suited for probing the thermodynamic trans influence because (i) any directional influence brought by partially filled d-block orbitals is removed, (ii) the transmission of interligand effects through the metallic center may occur via the empty 4s orbital,[23] and (iii) rapid thermodynamic chemical equilibria are ensured.

EXPERIMENTAL SECTION

Chemicals were purchased from Strem, Acros, Fluka AG, and Aldrich, and were used without further purification unless otherwise stated. The ligands **L1**,[15] **L2**,[15] and **L6**[22a] were prepared according to literature procedures. The synthesis of ligand **L7** is reported in Appendix 3 (Supporting Information). Acetonitrile and dichloromethane were distilled over calcium hydride. Silica gel plates Merck 60 F_{254} were used for thin-layer chromatography (TLC), and Fluka silica gel 60 (0.04−0.063 mm) or Acros neutral activated alumina (0.050−0.200 mm) was used for preparative column chromatography.

Preparation of *N*-5-Dimethyl-*N*-(2-nitrophenyl)pyrazine-2-carboxamide (7-H). 5-Methyl-2-pyrazinecarboxylic acid (**5**, 1.50 g, 10.9 mmol) and diisopropylethylamine (1.55 g, 12.0 mmol) in dichloromethane (5 mL) were added dropwise into a cooled (0 °C) solution of isobutylchloroformate (1.63 g, 12.0 mmol, 1.1 equiv) in dry dichloromethane (5 mL). The mixture was stirred for 30 min at 0 °C to give **6** in situ. *N*-Methyl-2-nitroaniline (**3**-H, 2.04 g, 14.1 mmol) in dichloromethane (10 mL) was slowly added, and the resulting solution was refluxed for 12 h. The solvent was evaporated. The viscous residue was dissolved in ethanol (20 mL) containing aqueous (aq) 0.2 M sodium hydroxide (20 mL), stirred vigorously for 30 min, and neutralized with aq 1.0 M hydrochloric acid. Evaporation to dryness provided a solid, which was partitioned between dichloromethane (40 mL) and aq half saturated NH_4Cl (40 mL). The organic layer was separated, and the aq phase was extracted with dichloromethane (3 × 30 mL). The combined organic phases were dried over anhydrous Na_2SO_4, filtered, and evaporated to dryness. The crude product was purified by flash column chromatography (silica gel; CH_2Cl_2/CH_3OH = 100:0 → 98.5:1.5) to give **7**-H as a beige solid (1.25 g, 4.6 mmol, yield 43%). ^{1}H NMR ($CDCl_3$, 400 MHz, only the major (85%) rotamer is described) δ/ppm: 8.92 (1H, s), 7.96 (1H, dd, ^3J = 8.2 Hz, ^4J = 1.4 Hz), 7.93 (1H, s), 7.53 (1H, td, ^3J = 7.6 Hz, ^4J = 1.6 Hz), 7.41 (1H, td, ^3J = 7.9 Hz, ^4J = 1.2 Hz), 7.28 (1H, dd, ^3J = 8.0 Hz, ^4J = 1.2 Hz), 3.49 (3H, s), 2.46 (3H, s). ESI-MS (CH_3OH): *m*/*z* 273.4 [(7-H)+H]$^+$, 295.4 [(7-H)+Na]$^+$.

The same procedure was used for the preparation of *N*-ethyl-5-methyl-*N*-(2-nitrophenyl)pyrazine-2-carboxamide (7-Me, yield 41%) by using *N*-ethyl-2-nitroaniline (**3**-Me). ^{1}H NMR ($CDCl_3$, 400 MHz, only the major (87%) rotamer is described) δ/ppm: 8.92 (1H, d, ^4J = 1.2 Hz), 7.96 (1H, dd, ^3J = 8.0 Hz, ^4J = 1.6 Hz), 7.93 (1H, d, ^4J = 0.8 Hz), 7.54 (1H, td, ^3J = 7.6 Hz, ^4J = 1.6 Hz), 7.42 (1H, td, ^3J = 7.8 Hz, ^4J = 1.5 Hz), 7.28 (1H, dd, ^3J = 7.8 Hz, ^4J = 1.4 Hz), 4.26 (1H, sex, ^2J = 14.0 Hz, ^3J = 7.1 Hz), 3.68 (1H, sex, ^2J = 14.0 Hz, ^3J = 6.9 Hz), 2.45 (3H, s), 1.26 (3H, t, ^3J = 7.2 Hz). ESI-MS (CH_3OH): *m*/*z* 287.1 [(7-Me)+H]$^+$, 303.9 [(7-Me)+Na]$^+$.

Preparation of *N*-Ethyl-2-(5-methylpyrazin-2-yl)-benzimidazole (L4). *N*-Ethyl-5-methyl-*N*-(2-nitrophenyl)pyrazine-2-carboxamide (7-Me, 2.86 g, 10 mmol) and sodium dithionite $Na_2S_2O_4$ (8.00 g, 40 mmol, 85% purity) were heated at 80 °C in ethanol (20 mL) and *N*,*N*-dimethylformamide (25 mL). Hot distilled water (20 mL) was added, and the mixture was refluxed for 24 h.

dx.doi.org/10.1021/ic5022559 | Inorg. Chem. 2014, 53, 13093−13104

Aqueous 4 M NaOH (10 mL) was slowly poured into the cooled solution, and the solvent was evaporated. The solid residue was partitioned between dichloromethane (200 mL) and water (100 mL). The organic layer was separated, washed with water (3 × 100 mL), dried over anhydrous Na_2SO_4, filtered, and evaporated to dryness. The crude product was purified by flash column chromatography (silica gel; CH_2Cl_2/CH_3OH = 98:2) to give **L4** as a white solid (1.20 g, 5.0 mmol, yield 51%). ^{1}H NMR ($CDCl_3$, 400 MHz) δ/ppm: 9.54 (1H, d, ^5J = 1.2 Hz), 8.52 (1H, d, ^5J = 0.4 Hz), 7.87−7.85 (1H, m), 7.48−7.46 (1H, m), 7.38−7.31 (2H, m), 4.80 (2H, q, ^3J = 7.2 Hz), 2.66 (3H, s), 1.49 (3H, t, ^3J = 7.2 Hz). ^{13}C NMR ($CDCl_3$, 100 MHz) δ/ppm: 153.48 (C_q), 147.45 (C_q), 144.94 (CH), 143.39 (C_q), 142.76 (C_q), 142.62 (CH), 136.17 (C_q), 123.65 (CH), 122.86 (CH), 120.29 (CH), 109.94 (CH), 40.49 (CH_2), 21.6 (CH_3), 15.39 (CH_3). ESI-MS (CH_3OH): m/z 239.4 [**L4**+H]$^+$. Anal. Calcd for $C_{14}H_{14}N_4$, C 70.57, H 5.92, N 23.51; found C 70.43, H 5.91, N 23.68%.

The same procedure was used for the preparation of *N*-methyl-2-(5-methylpyrazin-2-yl)benzimidazole (**L3**, yield 51%) by using *N*-5-dimethyl-*N*-(2-nitrophenyl)pyrazine-2-carboxamide (7-H). ^{1}H NMR ($CDCl_3$, 400 MHz) δ/ppm: 9.53 (1H, d, ^5J = 1.2 Hz), 8.52 (1H, d, ^5J = 0.8 Hz), 7.88−7.85 (1H, m), 7.47−7.44 (1H, m), 7.40−7.32 (2H, m), 4.25 (3H, s), 2.67 (3H, s). ^{13}C NMR ($CDCl_3$, 100 MHz) δ/ppm: 153.54 (C_q), 148.06 (C_q), 144.99 (CH), 143.31 (C_q), 142.63 (C_q), 142.42 (CH), 137.19 (C_q), 123.69 (CH), 122.91 (CH), 120.22 (CH), 109.87 (CH), 32.59 (CH_3), 21.61 (CH_3). ESI-MS (CH_3OH): m/z 225.4 [**L3**+H]$^+$. Anal. Calcd for $C_{13}H_{12}N_4$, C 69.92, H 5.39, N 24.98; found C 69.54, H 5.32, N 25.13%.

Slow diffusion of *n*-hexane into concentrated solutions of **L1** or **L3** in ethanol/dichloromethane (1:1) gave X-ray quality prisms for **L1** and needles for **L3**.

Preparation of the Complexes $[Zn(Lk)_n](CF_3SO_3)_2$ (Lk = L1, L3; *n* = 2−3). Stoichiometric amounts of **L1** or **L3** (3.0 equiv) and $Zn(CF_3SO_3)_2$ (28.1 mg, 0.08 mol, 1.0 equiv) were stirred for 30 min in acetonitrile (5 mL). Slow diffusion of diethyl ether provided $[Zn(\mathbf{L1})_3](CF_3SO_3)_2$ (yield 93%) and $[Zn(\mathbf{L3})_3](CF_3SO_3)_2$ (yield 92%) as white and pale yellow, respectively, microcrystalline powders.

$[Zn(\mathbf{L1})_3](CF_3SO_3)_2$. ^{1}H NMR ($CD_3CN$, 400 MHz, 333 K) δ/ppm: 8.26 (1H, d, ^3J = 8.4 Hz), 8.06 (1H, dd, ^3J = 8.2 Hz, ^4J = 1.4 Hz), 8.02 (1H, bs), 7.65 (1H, d, ^3J = 8.4 Hz), 7.42 (1H, ddd, ^3J = 8.4 Hz, ^3J = 7.2 Hz, ^4J = 0.8 Hz), 7.09 (1H, t, ^3J = 7.8 Hz), 6.68 (1H, d, ^3J = 8.0 Hz), 4.09 (3H, s), 2.30 (3H, s). ^{1}H NMR (CD_3NO_2, 400 MHz, 333 K) δ/ppm: 8.34 (1H, d, ^3J = 8.4 Hz), 8.17 (1H, bs), 8.09 (1H, d, ^3J = 8.4 Hz), 7.64 (1H, d, ^3J = 8.4 Hz), 7.41 (1H, ddd, ^3J = 8.4 Hz, ^3J = 7.6 Hz, ^4J = 1.2 Hz), 7.09 (1H, t, ^3J = 7.6 Hz), 6.76 (1H, bs), 4.16 (3H, bs), 2.67 (3H, s). Anal. Calcd for $C_{44}H_{39}F_6N_9O_6S_2Zn$, C 51.14, H 3.80, N 12.20; found C 50.76, H 3.83, N 12.15%.

$[Zn(\mathbf{L3})_3](CF_3SO_3)_2$. ^{1}H NMR ($CD_3CN$, 400 MHz, 323 K) δ/ppm: 9.51 (1H, d, ^5J = 1.2 Hz), 7.98 (1H, d, ^5J = 1.2 Hz), 7.72 (1H, d, ^3J = 8.4 Hz), 7.47 (1H, ddd, ^3J = 8.4 Hz, ^3J = 7.2 Hz, ^4J = 0.8 Hz), 7.15 (1H, ddd, ^3J = 8.4 Hz, ^3J = 7.2 Hz, ^4J = 0.8 Hz), 6.78 (1H, d, ^3J = 8.0 Hz), 4.26 (3H, s), 2.56 (3H, s). ^{1}H NMR (CD_3NO_2, 400 MHz, 333 K) δ/ppm: 9.57 (1H, d, ^5J = 1.2 Hz), 8.13 (1H, s), 7.72 (1H, d, ^3J = 8.4 Hz), 7.47 (1H, ddd, ^3J = 8.4 Hz, ^3J = 7.2 Hz, ^4J = 1.2 Hz), 7.13 (1H, ddd, ^3J = 8.0 Hz, ^3J = 7.2 Hz, ^4J = 0.8 Hz), 6.82 (1H, d, ^3J = 8.4 Hz), 4.33 (3H, s), 2.50 (3H, s). Anal. Calcd for $C_{41}H_{36}F_6N_{12}O_6S_2Zn$, C 47.52, H 3.50, N 16.22; found C 47.33, H 3.54, N 16.18%.

Slow diffusion of diethyl ether into concentrated nitromethane solutions provided X-ray quality prisms of $[Zn(\mathbf{L1})_3](CF_3SO_3)_2(H_2O)_{0.5}$ and $[Zn(\mathbf{L3})_3](CF_3SO_3)_2$. Slow diffusion of diethyl ether into concentrated acetonitrile solution containing **L1** or **L3** (1 equiv) and $Zn(CF_3SO_3)_2$ (1 equiv) gave small amounts of X-ray quality prisms of $[Zn(\mathbf{L1})_2(CF_3SO_3)(OH_2)](CF_3SO_3)(CH_3CN)$ and $[Zn(\mathbf{L3})_2(CF_3SO_3)_2](CH_3CN)$.

Spectroscopic and analytic measurements: ^{1}H and ^{13}C NMR spectra were recorded on a Bruker Avance 400 MHz spectrometer equipped with a variable-temperature unit. Chemical shifts were given in ppm with respect to tetramethylsilane $Si(CH_3)_4$. Pneumatically assisted electrospray ionization (ESI) mass spectra were recorded from 10^{-4} M solutions on an Applied Biosystems API 150EX LC/MS System equipped with a Turbo Ionspray source. Elemental analyses were performed by K. L. Buchwalder from the Microchemical Laboratory of the University of Geneva. Electronic absorption spectra in the UV−vis range were recorded at 20 °C from solutions with a PerkinElmer Lambda 900 spectrometer using quartz cells of 10 or 1 mm path length. Spectrophotometric titrations were performed with a J&M diode array spectrometer (Tidas series) connected to an external computer. In a typical experiment, 50 cm^3 of ligand in acetonitrile (2×10^{-4} mol·dm^{-3}) were titrated at 298 K with a solution of $Zn(CF_3SO_3)_2$ (2×10^{-3} mol·dm^{-3}) in acetonitrile under an inert atmosphere. After each addition of 0.15 mL, the absorbance was recorded using a Hellma optrode (optical path length 0.1 cm) immersed in the thermostated titration vessel and connected to the spectrometer. Mathematical treatment of the spectrophotometric titrations was performed with factor analysis and with the SPECFIT program.[24] Optimized gas-phase geometries (MM2 force field) and EHMO calculations for the ligands **L1** and **L3** were obtained from the softwares implemented in Chem3D Pro (PerkinElmer version 13.0.2.3021), http://www.cambridgesoft.com.

X-ray Crystallography. Summary of crystal data, intensity measurements, and structure refinements for **L1**, **L3**, **L5**, $[Zn(\mathbf{L1})_3](CF_3SO_3)_2(H_2O)_{0.5}$, $[Zn(\mathbf{L3})_3](CF_2SO_3)_2$ $[Zn(\mathbf{L1})_2(CF_3SO_3)(OH_2)](CF_3SO_3)(CH_3CN)$, $[Zn(\mathbf{L3})_2(CF_3SO_3)_2](CH_3CN)$, and $[EuZn(\mathbf{L7})_3](CF_3SO_3)_5(H_2O)_3(CH_3OH)(CH_3CN)_{0.5}$ were collected in Tables S1, S7, S12, and S17 (Supporting Information). The crystals were mounted on quartz fibers with protection oil. Several diffractometers were used to perform the X-ray data collections: an Agilent SuperNova Dual diffractometer equipped with a CCD Atlas detector for the samples measured with Cu Kα radiation, a Stoe IPDS 2 diffractometer equipped with an image plate for the samples measured with Mo Kα radiation, and a KUMA KM6-CH diffractometer equipped with a CCD detector for the sample measured with a wavelength λ = 0.699 71 Å at the Swiss Norwegian BeamLine (BM01A at the European Synchrotron Radiation Facility). The structures were solved by using direct methods.[25] Full-matrix least-squares refinements on F^2 were performed with SHELX97[26] or with CRYSTALS.[27] In the zinc complexes, some noncoordinated triflate anions were disordered, which limited the quality of the diffraction data. For $[Zn(\mathbf{L3})_3](CF_2SO_3)_2$, the Zn atom, located on the 2-fold axes (special position 4e), was six-coordinated by three didentate units corresponding to 100% of the *mer*-$[Zn(\mathbf{L3})_3]$ isomer. One ligand (labeled C, see Supporting Information, Figure S25) was disordered by rotation along the 2-fold axis with occupancy factors of 0.5 and refined with isotropic *U* parameters. The two other ligands (strands A and A#1) were related each other by the crystallographic 2-fold axis. One triflate anion in the asymmetric unit was located on a general position (8f).

RESULTS AND DISCUSSION

Synthesis and Molecular and Electronic Structures of the Didentate Ligands L1−L4. The preparation of ligands **L1**−**L4** exploits the reductive cyclization of aromatic ortho-nitrocarboxamides[28] for the connection of a benzimidazole ring at the 2-position of the pyridine ring in **L1** and **L2** (Scheme 2a),[15] or of the pyrazine ring in **L3** and **L4** (Scheme 2b). The activation of the 5-methyl-2-pyrazinecarboxylic acid **5** into its acyl chloride proved to be problematic. Reaction with oxalyl chloride or with thionyl chloride as chlorinating agents produced the target monocarboxamide synthon **7** together with considerable amounts of the oxidized dicarboxamide adducts **8** (Scheme 2b and Appendix 1 in the Supporting Information). The X-ray crystal structures of the cyclized final derivatives **L3** and **L5** ultimately confirmed the operation of this competitive pathway (Figure 2). Milder anhydride activation using isobutylchloroformate[29] eventually gave the monocarboxamide 7 in fair yields (Scheme 2b, right-hand side), which was transformed into the pyrazine-benzimidazole ligands

dx.doi.org/10.1021/ic5022559 | Inorg. Chem. 2014, 53, 13093−13104

Scheme 2[a]

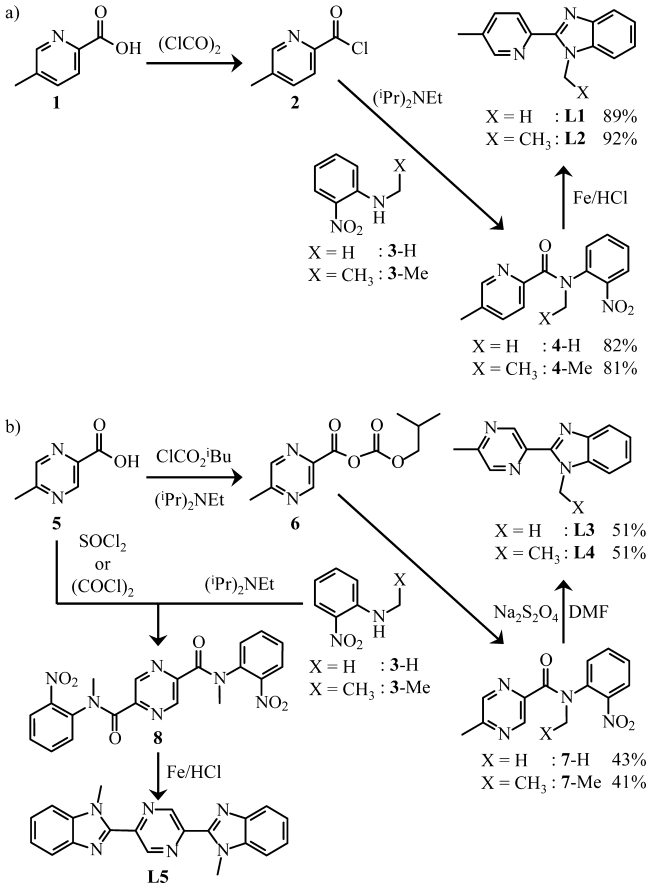

[a]Syntheses of the didentate ligands (a) **L1** and **L2** and (b) **L3** and **L4**. The unexpected reactivity of **5** with $SOCl_2$ or $(COCl)_2$ to give the side products **8** and **L5** is highlighted.

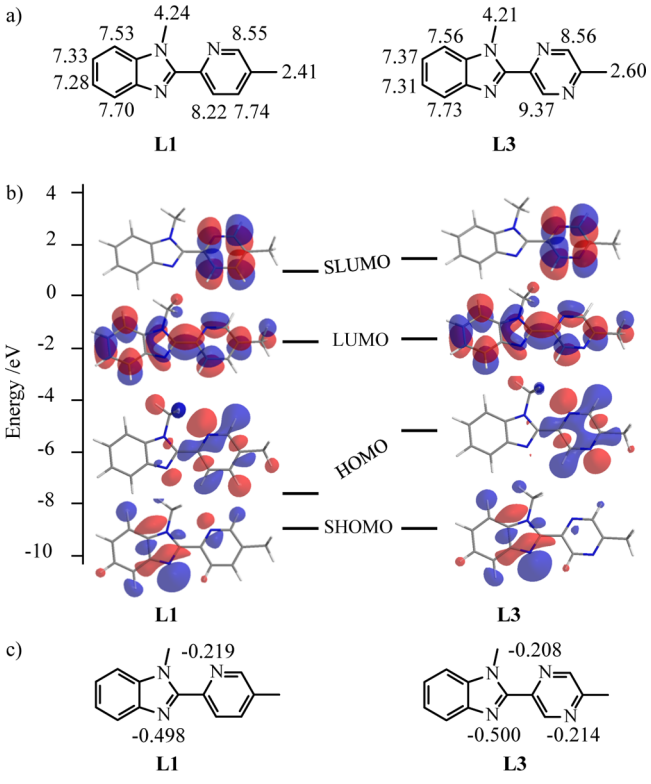

Figure 3. Electronic properties of the didentate ligands **L1** and **L3**. (a) ^{1}H NMR chemical shifts measured in CD_3CN, (b) extended Hückel computed frontier orbitals (optimized gas-phase models), and (c) computed charges (in electrostatic units) borne by the nitrogen donor atoms.

L3 and **L4** by using sodium dithionite as the reducing agent (Scheme 2b).[30]

The crystal structures of **L1** and **L3** may be superimposed (Figure S1 in the Supporting Information) and show quasi-coplanar benzimidazole−pyridine (interplanar angle = 3.5°) and benzimidazole−pyrazine (interplanar angle = 1.8°) didentate ligands adopting the trans conformation of the two nitrogen atoms bearing the electronic lone pairs, which minimizes both electronic charge repulsions and steric interactions (Figure 2 and Tables S1−S5 in the Supporting Information).[31]

The unusual downfield ^{1}H NMR shifts measured for the hydrogen atoms bound to C10 in **L1** (δ = 8.22 ppm) or to C16 in **L3** (δ = 9.37 ppm) are diagnostic for the preservation of the trans conformation of the α,α'-diimine units in solution, which puts the electronegative coordinating nitrogen atoms of the benzimidazole ring close to a hydrogen atom of the adjacent

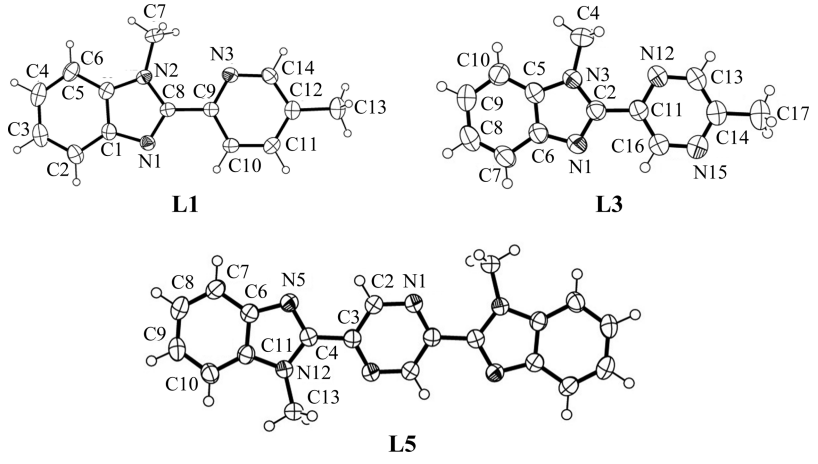

Figure 2. ORTEP views of the molecular structures of **L1**, **L3**, and **L5** with numbering schemes. Thermal ellipsoids are drawn at the 50% probability level.

dx.doi.org/10.1021/ic5022559 | Inorg. Chem. 2014, 53, 13093−13104

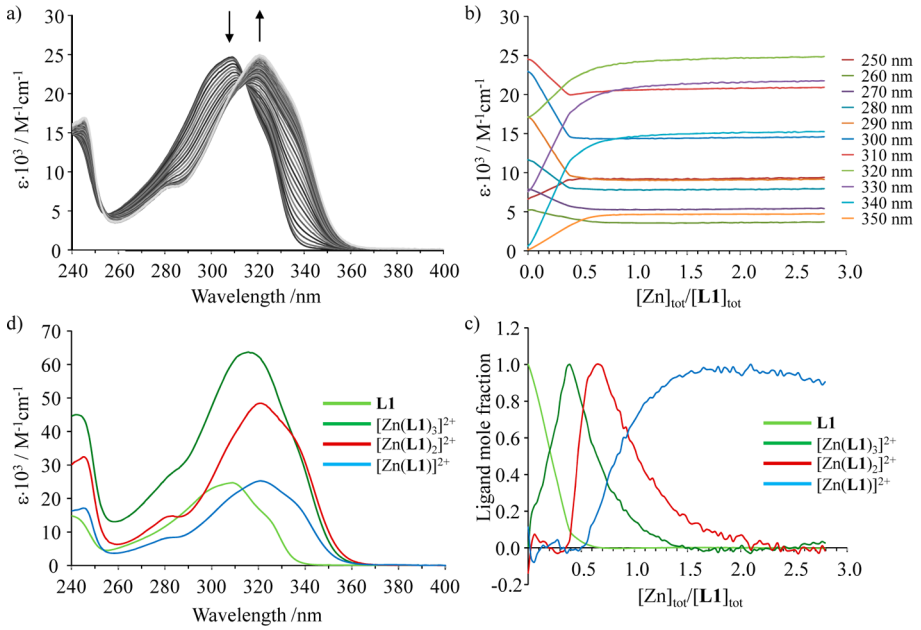

Figure 4. (a) Variation of absorption spectra and (b) corresponding variation of observed molar extinctions at different wavelengths observed for the spectrophotometric titration of **L1** with $Zn(CF_3SO_3)_2$ (total ligand concentration: 2×10^{-4} mol·dm^{-3} in acetonitrile, 298 K). (c) Evolving factor analysis using four absorbing eigenvectors[33] and (d) reconstructed individual electronic absorption spectra.[24]

Table 1. Thermodynamic Formation Constants Obtained from the Spectrophotometric Titrations of L1−L4 with MX_2 in Acetonitrile at 298 K (M = Fe(II), Co(II), Zn(II); X = $CF_3SO_3^-$, ClO_4^-)

ligand	M(II)	anion	$\log(\beta_{1,1}^{M,Lk})$	$\log(\beta_{1,2}^{M,Lk})$	$\log(\beta_{1,3}^{M,Lk})$	reference
L1	Zn	$CF_3SO_3^-$	7.7(7)	15.1(9)	22(1)	this work
L1	Zn	$CF_3SO_3^-$	7.8(2)	15.6(3)	22.7(4)	34
L1	Co	ClO_4^-	7.8(1)	14.9(2)	21.2(3)	35
L1	Fe	ClO_4^-	6.4(2)	12.2(3)	17.6(3)	35
L2	Zn	$CF_3SO_3^-$	5.88(8)	11.4(1)	16.6(1)	this work
L3	Zn	$CF_3SO_3^-$	6.9(1)	12.7(2)	17.6(2)	this work
L4	Zn	$CF_3SO_3^-$	4.8(1)	10.2(1)	14.5(2)	this work

pyridine/pyrazine ring (Figure 3a).[32] The similarity of the remaining part of the ^{1}H NMR spectra recorded for the two ligands indicates comparable electronic distributions within the aromatic rings (Figure 3a and Figure S2 in the Supporting Information). Extended Hückel calculations obtained for the ligands **L1** and **L3** in their optimized gas-phase geometries confirm this trend (Figure 3b). The only noticeable difference concerns the predicted reduction of the highest occupied molecular orbital−lowest unoccupied molecular orbital (HOMO−LUMO) gap in **L3** (Figure 3b), which is experimentally confirmed by a 1500 cm^{-1} red shift of the envelope of the $^1\pi^* \leftarrow {}^1\pi$ electronic transitions observed in the absorption spectra in going from **L1** to **L3** (Figure S3 in the Supporting Information). Finally, the computed partial negative charge borne by the coordinating nitrogen atoms slightly decreases in going from 2-pyridine-benzimidazole (**L1**) to 2-pyrazine-benzimidazole (**L3**, Figure 3c).

To summarize, the replacement of the pyridine ring found in **L1** and **L2** with a pyrazine ring in **L3** and **L4** does not significantly affect the structural and electronic parameters of the didentate chelates. The main difference concerns the 5% increase in the charge difference between the two coordinating nitrogen atoms in the presence of a pyrazine ring. This improves the push−pull character of the chelating unit in **L3** and **L4**, hence the potential thermodynamic trans influence according to ref 17b.

Thermodynamic Complexation of Ligands L1−L4 with $Zn(CF_3SO_3)_2$. The spectrophotometric titrations of **L1**−**L4** with $Zn(CF_3SO_3)_2$ in dry acetonitrile show the successive formation of three absorbing complexes characterized by smooth end points at Zn/**Lk** = 1:3, Zn/**Lk** = 1:2, and Zn/**Lk** = 1:1 (Figure 4a,b and Supporting Information, Figures S4a,b−S6a,b). Factor analysis (Figure 4c and Supporting Information, Figures S4c−S6c)[33] followed by nonlinear least-squares fits[24] to equilibria 2−4 provide satisfying reconstructed individual absorption spectra (Figure 4d and Supporting Information, Figures S4d−S6d) together with the macroscopic formation constants gathered in Table 1.

$$Zn^{2+} + \mathbf{Lk} \rightleftharpoons [Zn\mathbf{Lk}]^{2+} \beta_{1,1}^{Zn,Lk} \quad (2)$$

$$Zn^{2+} + 2\mathbf{Lk} \rightleftharpoons [Zn(\mathbf{Lk})_2]^{2+} \beta_{1,2}^{Zn,Lk} \quad (3)$$

$$Zn^{2+} + 3\mathbf{Lk} \rightleftharpoons [Zn(\mathbf{Lk})_3]^{2+} \beta_{1,3}^{Zn,Lk} \quad (4)$$

As expected, the complexes with the ethyl-substituted ligands **L2** and **L4** are destabilized by 2−5 orders of magnitude with respect to their methyl-substituted analogues **L1** and **L3** because the intraligand steric strain induced by the cis coordination of the didentate α,α'-diimine chelates puts the N substituent close to the hydrogen atom bound to the meta position of the central pyridine ring.[36] Within each pair of methyl- or ethyl-substituted ligands (i.e., the **L1**,**L3** and **L2**,**L4** pairs), the formation constants decrease upon replacement of the pyridine ring with a pyrazine ring, which is a trend in line with (i) the reduction of the proton affinity in going from a pyridine (pK_a = 5.23) to a pyrazine unit (pK_a = 0.65)[37] and (ii) the decrease of the total negative charge borne by the coordinating nitrogen atoms in the benzimidazole−pyrazine binding units (Figure 3c).

dx.doi.org/10.1021/ic5022559 | Inorg. Chem. 2014, 53, 13093−13104

Scheme 3[a]

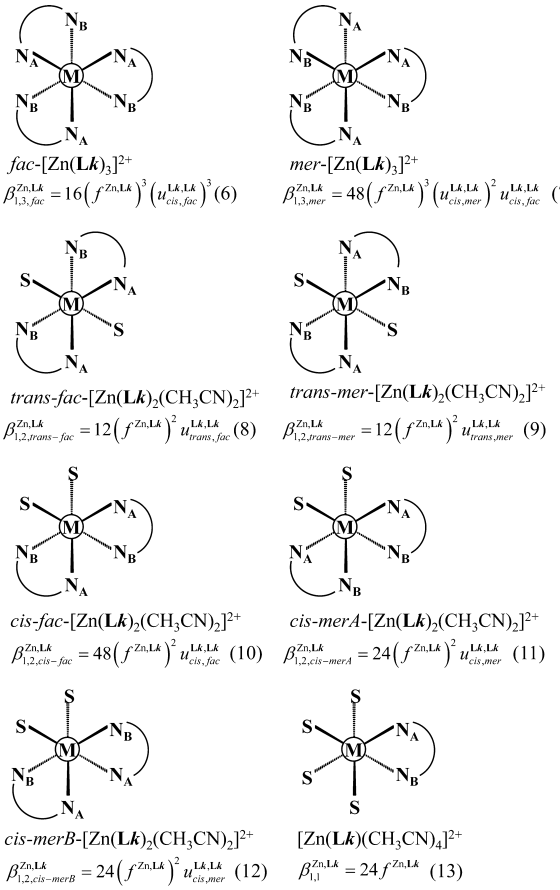

[a]Microspecies and associated microscopic formation constants considered for the complexes $[Zn(\mathbf{Lk})_3]^{2+}$ (eqs 6 and 7), $[Zn(\mathbf{Lk})_2(CH_3CN)_2]^{2+}$ (eqs 8−12), and $[Zn(\mathbf{Lk})(CH_3CN)_4]^{2+}$ (eq 13). For $[Zn(\mathbf{Lk})(CH_3CN)_2]^{2+}$, we use the cis/trans terminology for describing the relative orientation of the two solvent molecules, whereas the additional mer/fac designation refers to the relative orientation of the two unsymmetrical ligands as defined in the saturated $[Zn(\mathbf{Lk})_3]^{2+}$ complex; i.e., a trans N_A-Zn-N_A arrangement is noted merA, a trans N_B-Zn-N_B is noted merB, and a trans N_A-Zn-N_B is noted fac.

A deeper and quantitative analysis relies on the site binding model (eq 5),[38] which combines a statistical factor $K^{stat}_{1,m} = \omega^{chiral}_{1,m}\cdot\omega^{M,\mathbf{Lk}}_{1,m}$ with two microscopic chemical parameters $f^{M,\mathbf{Lk}}$ and $u^{\mathbf{Lk},\mathbf{Lk}}_{k,l}$ for modeling the thermodynamic formation constants of the purely intermolecular complexation processes described in the successive equilibria (2)−(4). The m subscripts stand for the number of ligands in the $[M(\mathbf{Lk})_m]$ complex.

$$\beta^{M,\mathbf{Lk}}_{1,m} = e^{-\Delta G^{M,\mathbf{Lk}}_{1,m}/RT} = K^{stat}_{1,m}\cdot K^{chem}_{1,m} = (\omega^{chiral}_{1,m}\cdot\omega^{M,\mathbf{Lk}}_{1,m})\cdot\left(\prod_{i=1}^{m} f^{M,\mathbf{Lk}}\cdot\prod_{k<l} u^{\mathbf{Lk},\mathbf{Lk}}_{k,l}\right) \quad (5)$$

The geometrical part of the statistical factor $\omega^{M,\mathbf{Lk}}_{1,m}$ takes into account the change in rotational entropy between the reactants and products, and it can be obtained by using the symmetry number method (Appendix 2).[39] The additional $\omega^{chiral}_{1,m}$ term accounts for the entropy of mixing of enantiomers, which appears when a molecule exists at equilibrium as a racemic mixture ($\omega^{chiral}_{1,m} = 1$ for reactions that do not create or remove chiral partners, and $\omega^{chiral}_{1,m} \neq 1$ otherwise).[8] The chemical part of the complexation process $K^{chem}_{1,m} = \prod_{i=1}^{m}(f^{M,\mathbf{Lk}}_i)\prod_{k<1}(u^{\mathbf{Lk},\mathbf{Lk}}_{k,l})$ has also two contributions. (1) The product $\prod_{i=1}^{m}(f^{M,\mathbf{Lk}}_i)$ collects the intermolecular microscopic affinities (including desolvation) characterizing the inner sphere connection of M(II) to each didentate binding site of **Lk** characterized by a $f^{M,\mathbf{Lk}}_i$ descriptor. (2) The term $\prod_{k<1}(u^{\mathbf{Lk},\mathbf{Lk}}_{k,l})$ stands for the product of the Boltzmann's factors $u^{\mathbf{Lk},\mathbf{Lk}}_{k,l} = e^{-(\Delta E^{\mathbf{Lk},\mathbf{Lk}}_{kj}/RT)}$ accounting for the interligand free energy of interactions $\Delta E^{\mathbf{Lk},\mathbf{Lk}}_{k,l}$, which operate when two ligands are bound to the same metal.[38] Let us consider *fac*-$[Zn(\mathbf{Lk})_3]^{2+}$ as a working example where the three didentate ligands act as cis partners (Scheme 3). First, the statistical factor is deduced by using the symmetry number methods and amounts to $K^{stat}_{1,3,fac} = 16$ (Supporting Information, Figure A2−1 in Appendix 2). Second, the chemical contribution takes into account thrice the connection of **Lk** to Zn(II) (i.e., $(f^{M,\mathbf{Lk}}_i)^3$) modulated by three possible pairs of interligand interactions, which corresponds to $(u^{\mathbf{Lk},\mathbf{Lk}}_{cis,fac})^3$. Altogether, the thermodynamic $\beta^{Zn,\mathbf{Lk}}_{1,3,fac}$ constant associated with the formation of the saturated facial isomer is thus modeled with eq 6.

$$\beta^{Zn,\mathbf{Lk}}_{1,3,fac} = 16(f^{Zn,\mathbf{Lk}})^3(u^{\mathbf{Lk},\mathbf{Lk}}_{cis,fac})^3 \quad (6)$$

Following this strategy, each microspecies contributing to eqs 2−4 is modeled with eqs 6−13 (Scheme 3), and the final thermodynamic macroconstant $\beta^{M,\mathbf{Lk}}_{1,m}$ considered in equilibria (2)−(4) are obtained by summing the pertinent microconstants to give eqs 14−16.

$$\beta^{Zn,\mathbf{Lk}}_{1,1} = 24f^{Zn,\mathbf{Lk}} \quad (14)$$

$$\beta^{Zn,\mathbf{Lk}}_{1,2} = 12(f^{Zn,\mathbf{Lk}})^2(u^{\mathbf{Lk},\mathbf{Lk}}_{trans,fac} + u^{\mathbf{Lk},\mathbf{Lk}}_{trans,mer} + 4u^{\mathbf{Lk},\mathbf{Lk}}_{cis,fac} + 4u^{\mathbf{Lk},\mathbf{Lk}}_{cis,mer}) \quad (15)$$

$$\beta^{Zn,\mathbf{Lk}}_{1,3} = 16(f^{Zn,\mathbf{Lk}})^3 u^{\mathbf{Lk},\mathbf{Lk}}_{cis,fac}[(u^{\mathbf{Lk},\mathbf{Lk}}_{cis,fac})^2 + 3(u^{\mathbf{Lk},\mathbf{Lk}}_{cis,mer})^2] \quad (16)$$

Table 2. Thermodynamic Microscopic Parameters Modelling the Complexation of L1−L4 with $Zn(CF_3SO_3)_2$ in Acetonitrile at 298 K (fit of eqs 14−16)

			$\Delta G^{Zn,\mathbf{Lk}}_{affinity}$ [a]		$\Delta E^{\mathbf{Lk},\mathbf{Lk}}$ [b]	
ligand	M(II)	$\log(f^{ZN,\mathbf{Lk}})$	kJ/mol	$\log(u^{\mathbf{Lk},\mathbf{Lk}})$	kJ/mol	AF[c]
L1	Zn	6.32(5)	−36.0(3)	0.40(5)	−2.3(3)	2.27×10^{-3}
L2	Zn	4.43(7)	−25.2(4)	0.49(9)	−2.8(5)	4.87×10^{-3}
L3	Zn	5.45(6)	−31.1(3)	−0.18(7)	1.0(4)	3.39×10^{-3}
L4	Zn	3.7(2)	−21(1)	0.6(3)	−3(2)	1.83×10^{-2}

[a]$\Delta G^{Zn,\mathbf{Lk}}_{affinity} = -RT\ln(f^{Zn,\mathbf{Lk}})$. [b]$\Delta E^{\mathbf{Lk},\mathbf{Lk}} = -RT\ln(u^{\mathbf{Lk},\mathbf{Lk}})$. [c]Agreement factor AF = $(\sum_{i=1}^{3}(\log\beta^{Zn,\mathbf{Lk}}_{1,i,exp} - \log\beta^{Zn,\mathbf{Lk}}_{1,i,calcd})^2/\sum_{i=1}^{3}(\log\beta^{Zn,\mathbf{Lk}}_{1,i,exp})^2)^{1/2}$.[40]

dx.doi.org/10.1021/ic5022559 | Inorg. Chem. 2014, 53, 13093−13104

Table 3. Thermodynamic Exchange Constants Obtained by NMR (at 233 K) and Spectrophotometric (at 298 K) Titrations of L1−L4 with $Zn(CF_3SO_3)_2$ in Acetonitrile and Extended Set of Thermodynamic Microscopic Parameters (fit of eqs 14−16, 19, and 20)[42]

	L1	L2	L3	L4
$\log(K_{exch}^{Zn,Lk})^a$	10.0(7)	10.3(6)	9(2)	22(1)
$\log(K_{exch}^{Zn,Lk})^b$	3(11)	2(1)	9(8)	14(9)
$\log(K_{mer\rightarrow fac}^{Zn,Lk})$	0.47(2)	0.27(1)	1.5(1)	0.88(3)
$\log(f^{Zn,Lk})$	6.3(2)	4.37(3)	5.49(5)	3.40(4)
$\Delta G_{affinity}^{Zn,Lk}$/kJ·mol^{-1} ^{c}	−36(1)	−24.9(2)	−31.3(3)	−19.4(2)
$\log(u_{trans}^{Lk,Lk})$	1.1(2)	1.26(2)	−8(2)	2.00(2)
$\Delta E_{trans}^{Lk,Lk}$/kJ·mol^{-1} ^{d}	−6(1)	−7.2(1)	44(13)	−11.4(1)
$\log(u_{cis,fac}^{Lk,Lk})$	0.5(1)	0.50(1)	−0.08(2)	0.90(1)
$\Delta E_{cis,fac}^{Lk,Lk}$/kJ·mol^{-1} ^{d}	−2.6(6)	−2.83(7)	0.5(1)	−5.12(8)
$\log(u_{cis,mer}^{Lk,Lk})$	0.4(1)	0.54(1)	−0.41(2)	0.69(1)
$\Delta E_{cis,mer}^{Lk,Lk}$/kJ·mol^{-1} ^{d}	−2.2(6)	−3.07(7)	2.3(1)	−3.92(8)
AF^e	7.9×10^{-3}	1.4×10^{-2}	8.2×10^{-4}	2.9×10^{-3}

^{a}Determined by integration of the ^{1}H NMR signals at 233 K. ^{b}Computed with $K_{exch}^{Zn,Lk} = (\beta_{1,2}^{Zn,Lk})^2/\beta_{1,1}^{Zn,Lk} \times \beta_{1,3}^{Zn,Lk}$ and using the formation constants determined by spectrophotometry at 298 K (Table 1). $^c\Delta G_{affinity}^{Zn,Lk} = -RT \ln(f^{Zn,Lk})$. $^d\Delta E^{Lk,Lk} = -RT \ln(u^{Lk,Lk})$. ^{e}Agreement factor AF = $(\sum_{i=1}^{5}(\log \beta_{i,exp} - \log \beta_{i,calcd})^2/\sum_{i=1}^{5}(\log \beta_{i,exp})^2)^{1/2}$ with $\beta_{i,exp}$ corresponding to the formation constants (eqs 14−16) or to the exchange constants (eqs 17 and 18).[40]

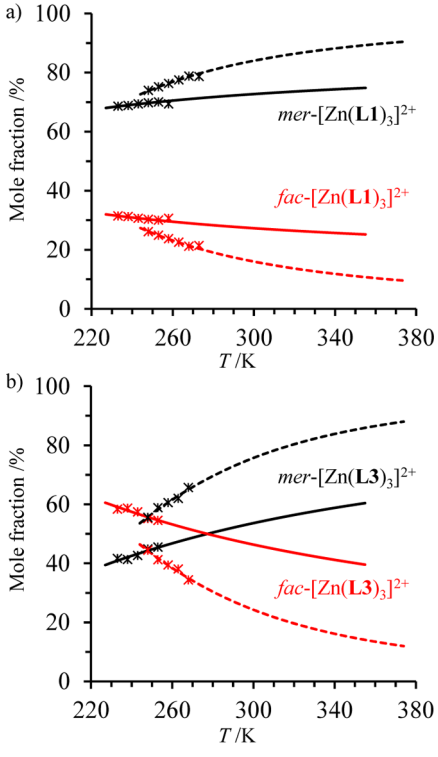

Figure 5. Variable-temperature speciation of *fac*-$[Zn(\mathbf{Lk})_3]^{2+}$ (red traces) and *mer*-$[Zn(\mathbf{Lk})_3]^{2+}$ (black traces) in CD_3CN (full trace) and CD_3NO_2 (dotted traces) for (a) **L1** and (b) **L3**. The experimental data are shown as stars, and the traces are computed trends using the van't Hoff equation $-RT \ln(K_{mer\rightarrow fac}^{Zn,Lk}) = \Delta H_{mer\rightarrow fac}^{Zn,Lk} - T\Delta S_{mer\rightarrow fac}^{Zn,Lk}$ within the accessible temperature range of each solvent.

Assuming the operation of a single average intermetallic interaction $u_{trans,fac}^{Lk,Lk} \simeq u_{trans,mer}^{Lk,Lk} \simeq u_{cis,fac}^{Lk,Lk} \simeq u_{cis,mer}^{Lk,Lk} \equiv u^{Lk,Lk}$, only two microscopic descriptors $f^{Zn,Lk}$ and $u^{Lk,Lk}$ are required for modeling the three macroscopic constants obtained by spectrophotometry. Linear least-squares fits provide the affinity parameters $\Delta G_{affinity}^{Zn,Lk} = -RT \ln(f^{Zn,Lk})$ and interligand interactions $\Delta E^{Lk,Lk} = -RT \ln(u^{Lk,Lk})$ gathered in Table 2, which satisfyingly reproduce the experimental data (Table 2 column 7 and Figure S7 in the Supporting Information).

In terms of free energy, the affinity of Zn(II) for the didentate unit decreases by 15(2)% upon replacement of the pyridine unit in **L1−L2** with a pyrazine unit in **L3−L4**. A 32(1)% reduction is observed within each pair of ligands when the methyl residue connected to the benzimidazole (bzim) ring is replaced with the sterically more demanding ethyl group. Though weak, the interligand interactions are globally cooperative ($\Delta E^{Lk,Lk} < 0$ except for a weak positive value found for **L3**), thus favoring the successive fixation of several didentate binding units to the central divalent zinc cation. Focusing on the Zn(II) coordination sphere, $\Delta E^{Lk,Lk} < 0$ suggests that the metal−ligand affinities should increase upon successive ligand binding, a prediction that contrasts with the stretching of the Zn−N bond lengths computed for $[Zn(\mathbf{L0})(H_2O)_4]^{2+}$ (2.107 Å) < $[Zn(\mathbf{L0})_2(H_2O)_2]^{2+}$ (2.147 Å) < $[Zn(\mathbf{L0})_3]^{2+}$ (2.218 Å) in water,[31] a trend experimentally confirmed in the solid state for $[Zn(\mathbf{Lk})_2]^{2+}$ (k = 1, 3; Zn−N_{bzim} = 2.081(8) Å, Zn−$N_{pyridine}$ = 2.16(2) Å, Zn−$N_{pyrazine}$ = 2.19(4) Å) and of $[Zn(\mathbf{Lk})_3]^{2+}$ (k = 1, 3; Zn−N_{bzim} = 2.10(5) Å, Zn−$N_{pyridine}$ = 2.24(4) Å, Zn−$N_{pyrazine}$ = 2.27(3) Å, vide infra). We therefore conclude that solvation effects overcome the intramolecular steric effects and control the thermodynamic interligand interactions operating in these charged complexes in solution.[41]

Microscopic Speciations of the $[Zn(Lk)_m]^{2+}$ Complexes in Solution (Lk = L1−L4 and m = 1−3). The ^{1}H NMR titrations of **L1−L4** with $Zn(CF_3SO_3)_2$ in CD_3CN confirm the successive formation of the three 1:3, 1:2, and 1:1 Zn/**Lk** complexes at 233 K, a temperature at which the dynamic exchange processes are blocked on the NMR time scale (Figures S8−S11 in the Supporting Information). The speciations determined by integration of the ^{1}H NMR signals at 233 K compare well with those predicted by using the macroconstants estimated by spectrophotometry (Figures S12−S15 in the Supporting Information) thus leading to a fair matching of the exchange constants $K_{exch}^{Zn,Lk}$ (eq 17) measured by NMR (Table 3, entry 1) and by spectrophotometry (in Table 3, entry 2). Interestingly, the amount of *fac*-$[Zn(\mathbf{Lk})_3]^{2+}$ and *mer*-$[Zn(\mathbf{Lk})_3]^{2+}$ microspecies can be addressed by NMR at 233 K (Supporting Information, Figures

dx.doi.org/10.1021/ic5022559 | Inorg. Chem. 2014, 53, 13093−13104

Table 4. Thermodynamic Enthalpic ($\Delta H^{Zn,Lk}_{mer\rightarrow fac}$) and Entropic ($\Delta S^{Zn,Lk}_{mer\rightarrow fac}$) Contributions to Equilibrium 18 in Solution

complex	solvent	ε_r [a]	$\Delta H^{Zn,Lk}_{mer\rightarrow fac}$ kJ/mol	$\Delta S^{Zn,Lk}_{mer\rightarrow fac}$ J/mol·K	$\Delta G^{Zn,Lk,\circ}_{mer\rightarrow fac}$ [b] kJ/mol	$K^{Zn,Lk}_{mer\rightarrow fac}$ [b]	reference
$[Co(\mathbf{L1})_3]^{2+}$	CD_3CN	37.5	0.6(3)	−10(1)	3.6(4)	0.24(9)	15
$[Zn(\mathbf{L1})_3]^{2+}$	CD_3CN	37.5	−1.7(1)	−14(1)	2.5(3)	0.4(1)	this work
$[Zn(\mathbf{L1})_3]^{2+}$	CD_3NO_2	35.9	−7.4(3)	−39(1)	4.2(4)	0.18(7)	this work
$[Zn(\mathbf{L3})_3]^{2+}$	CD_3CN	37.5	−4(1)	−16(4)	0.8(1.6)	0.7(1.0)	this work
$[Zn(\mathbf{L3})_3]^{2+}$	CD_3NO_2	35.9	−11(1)	−45(4)	2.4(1.5)	0.4(5)	this work

[a] Relative dielectric constants. [b] $\Delta G^{Zn,Lk,\circ}_{mer\rightarrow fac}$ and $K^{Zn,Lk}_{mer\rightarrow fac}$ are calculated at T = 298 K.

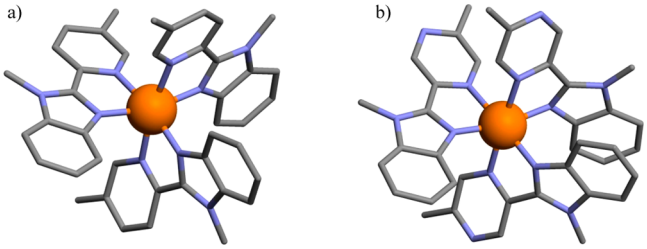

Figure 6. Perspective views of the molecular structures of the pseudo-octahedral cations (a) *mer*-$[Zn(\mathbf{L1})_3]^{2+}$ and (b) *mer*-$[Zn(\mathbf{L3})_3]^{2+}$ in the crystal structures of $[Zn(\mathbf{L1})_3](CF_3SO_3)_2(H_2O)_{0.5}$ and $[Zn(\mathbf{L3})_3](CF_2SO_3)_2$. Colors: gray = C atoms, blue = N atom, orange = Zn atom. H atoms are omitted for clarity.

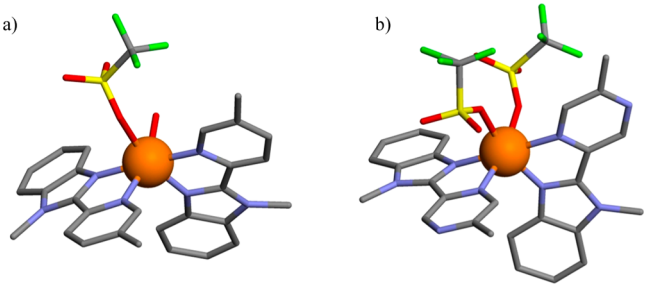

Figure 7. Perspective views of the molecular structures of pseudo-octahedral complexes (a) *cis-fac*-$[Zn(\mathbf{L1})_2(CF_3SO_3)(OH_2)]^+$ and (b) *cis-fac*-$[Zn(\mathbf{L3})_2(CF_3SO_3)_2]$ in the crystal structures of $[Zn(\mathbf{L1})_2(CF_3SO_3)(OH_2)](CF_3SO_3)(CH_3CN)$ and $[Zn(\mathbf{L3})_2(CF_3SO_3)_2](CH_3CN)$. Colors: gray = C atoms, blue = N atoms, red = O atoms, green = F atoms, yellow = S atoms, orange = Zn-atoms. H atoms are omitted for clarity.

S8−S11), which allows the quantification of the mer↔fac equilibria (18) (Table 3, entry 3).

$$[Zn(\mathbf{Lk})]^{2+} + [Zn(\mathbf{Lk})_3]^{2+} \rightleftharpoons 2[Zn(\mathbf{Lk})_2]^{2+} K^{Zn,Lk}_{exch} \quad (17)$$

$$mer\text{-}[Zn(\mathbf{Lk})_3]^{2+} \rightleftharpoons fac\text{-}[Zn(\mathbf{Lk})_3]^{2+} K^{Zn,Lk}_{mer\rightarrow fac} \quad (18)$$

Application of the site binding model (eq 5) to equilibria 17 and 18 gives eqs 19 and 20.

$$K^{Zn,Lk}_{exch} = \frac{(\beta^{Zn,Lk}_{1,2})^2}{\beta^{Zn,Lk}_{1,1}\cdot\beta^{Zn,Lk}_{1,3}} = \frac{3}{8}\cdot\frac{(u^{Lk,Lk}_{trans,fac} + u^{Lk,Lk}_{trans,mer} + 4u^{Lk,Lk}_{cis,fac} + 4u^{Lk,Lk}_{cis,mer})^2}{u^{Lk,Lk}_{cis,fac}[(u^{Lk,Lk}_{cis,fac})^2 + 3(u^{Lk,Lk}_{cis,mer})^2]} \quad (19)$$

$$K^{Zn,Lk}_{mer\rightarrow fac} = \frac{\beta^{Zn,Lk}_{1,3,fac}}{\beta^{Zn,Lk}_{1,3,mer}} = \frac{1}{3}\cdot\left(\frac{u^{Lk,Lk}_{cis,fac}}{u^{Lk,Lk}_{cis,mer}}\right)^2 \quad (20)$$

A global nonlinear least-squares fit[42] of the thermodynamic data gained by NMR (eqs 19 and 20) and by spectrophotometry (eqs 14−16) provides the extended set of four microscopic thermodynamic descriptors $f^{Zn,Lk}$, $u^{Lk,Lk}_{cis,fac}$, $u^{Lk,Lk}_{cis,mer}$, and $u^{Lk,Lk}_{trans,fac} \simeq u^{Lk,Lk}_{trans,mer} \equiv u^{Lk,Lk}_{trans}$ gathered in Table 3 (entries 4−11), from which the comprehensive microspeciations can be computed (Table S6 and Figures S16−S19 in the Supporting Information).

The affinity of Zn(II) for the didentate unit ($-36 \le \Delta G^{Zn,Lk}_{affinity} \le -19$ kJ/mol; entry 5 in Table 3) represents the predominant driving force of the complexation processes, closely followed by the interligand interaction $\Delta E^{Lk,Lk}_{trans}$, which operates when two coordinated ligands are coplanar (entry 7 in Table 3). Though weaker in magnitude, the interactions occurring between noncoplanar ligands $\Delta E^{Lk,Lk}_{cis,mer}$ and $\Delta E^{Lk,Lk}_{cis,fac}$ measure the thermodynamic trans influence (entries 9 and 11 in Table 3). In absence of trans influence, $\Delta E^{Lk,Lk}_{cis,mer} = \Delta E^{Lk,Lk}_{cis,fac}$, and the ratio *fac*-$[Zn(\mathbf{Lk})_3]^{2+}$/*mer*-$[Zn(\mathbf{Lk})_3]^{2+}$ amounts to 1/3 (eq 20).[19] This situation holds for the pyridine−benzimidazole ligands **L1** and **L2**, whereas $\Delta E^{Lk,Lk}_{cis,mer} > \Delta E^{Lk,Lk}_{cis,fac}$ observed for the pyrazine−benzimidazole units **L3** and **L4** is diagnostic for the operation of a weak trans influence favoring the formation of *fac*-$[Zn(\mathbf{L3})_3]^{2+}$ and *fac*-$[Zn(\mathbf{L4})_3]^{2+}$, in which three trans $N_{pyrazine}-Zn-N_{benzimidazole}$ correlations exist (see Figure 1). The computed energy differences $\Delta E^{Lk,Lk}_{cis,mer} - \Delta E^{Lk,Lk}_{cis,fac}$ = 1.8(1) kJ/mol for **L3** and 1.2(1) kJ/mol for **L4** translate into 60(2)% and 47(1)% mole fractions of the *fac*-$[Zn(\mathbf{L3})_3]^{2+}$ and *fac*-$[Zn(\mathbf{L4})_3]^{2+}$ complexes in acetonitrile solution at 233 K (Figure 5b), instead of the proportion of 25% expected under statistical conditions (Figure 5a).

Thermodynamics of $[Zn(Lk)_3]^{2+}$ Meridional/Facial Isomerization in Solution (Lk = L1, L3). Variable-temperature ^1H NMR speciations of $[Zn(\mathbf{Lk})_3]^{2+}$ in the 233−333 K range obey the van't Hoff equation $\Delta G^{Zn,Lk}_{mer\rightarrow fac} = -RT\ln(K^{Zn,Lk}_{mer\rightarrow fac}) = \Delta H^{Zn,Lk}_{mer\rightarrow fac} - T\Delta S^{Zn,Lk}_{mer\rightarrow fac}$, and linear plots of $\ln(K^{Zn,Lk}_{mer\rightarrow fac})$ versus T^{-1} provide the enthalpic and entropic contributions to eq 18 (Table 4 and Supporting Information, Figures S20−S24). The free energy changes at room temperature $0.8 \le \Delta G^{Zn,Lk,\circ}_{mer\rightarrow fac} \le 4.2$ kJ·mol^{-1} are close to the statistical contribution $\Delta G^{mer\rightarrow fac}_{exch,stat} = -T\Delta S^{mer\rightarrow fac}_{exch,stat} = -RT\ln(1/3) = 2.7$ kJ·mol^{-1},[19] which ensures the predominance of the meridional isomers at 298 K (Figure 5). However, the opposite enthalpic and entropic contributions to the free energy changes for both $[Zn(\mathbf{L1})_3]^{2+}$ and $[Zn(\mathbf{L3})_3]^{2+}$ point to partial reversal at low temperature (Figure 5).

The enthalpic driving force favors the facial isomer in agreement with the operation of the trans influence at the molecular level for both complexes. However, the significant

dx.doi.org/10.1021/ic5022559 | Inorg. Chem. 2014, 53, 13093−13104

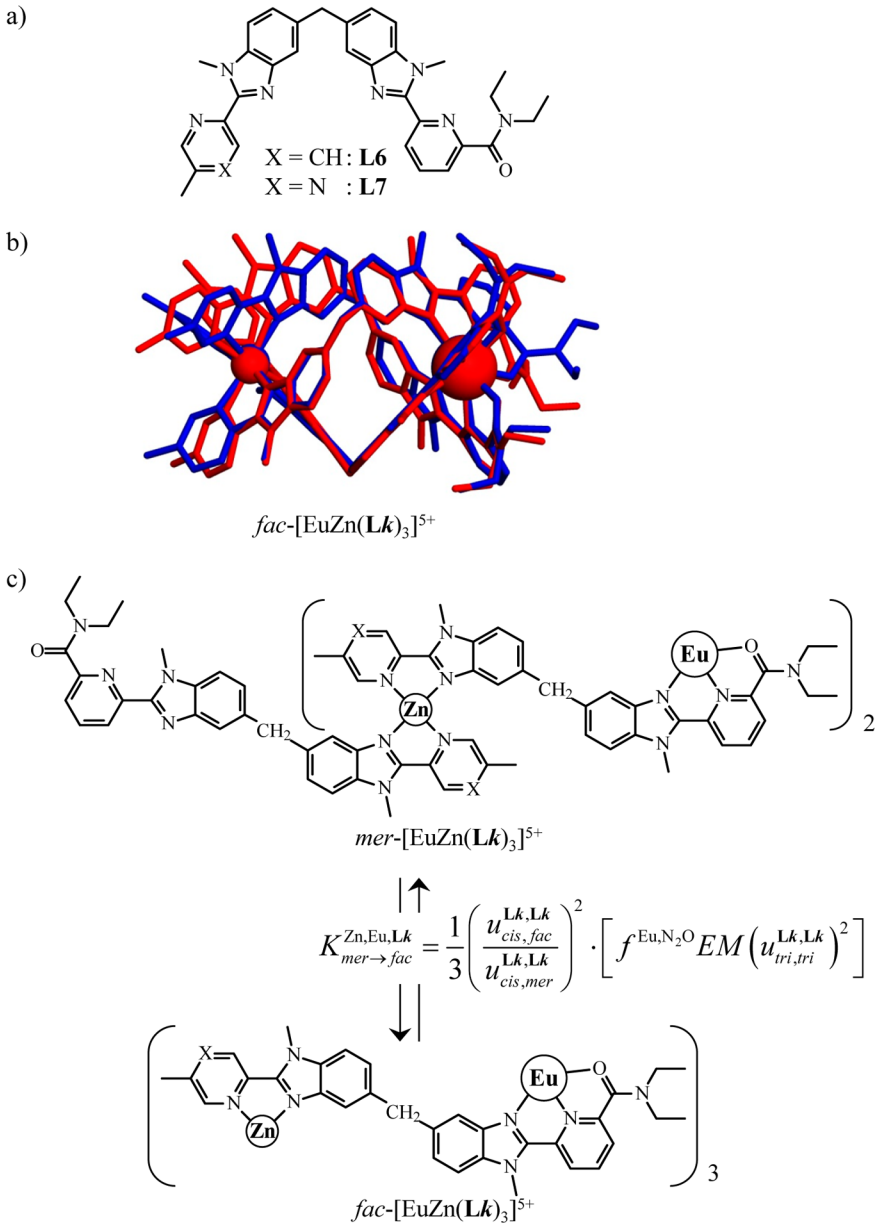

Figure 8. (a) Chemical structure of the segmental ligands **L6** and **L7**, (b) superimposition of the molecular structures of $[EuZn(\mathbf{L6})_3]^{5+}$ (red) and $[EuZn(\mathbf{L7})_3]^{5+}$ (blue) in the crystal structures of $[EuZn(\mathbf{L6})_3](ClO_4)(CF_3SO_3)_4(CH_3CN)_4$[22a] and $[EuZn(\mathbf{L7})_3](CF_3SO_3)_5(H_2O)_3(CH_3OH)(CH_3CN)_{0.5}$, and (c) thermodynamic equilibrium showing the meridional to facial isomerization in the dinuclear $[EuZn(\mathbf{Lk})_3]^{5+}$ complexes.

variation of $\Delta H^{Zn,Lk}_{mer\rightarrow fac}$ measured for the same complexes in acetonitrile and in nitromethane suggests that solvation processes play a crucial role in the mer↔fac isomerization process. Since the electric dipole moment of the C_3-symmetrical facial isomer *fac*-$[Zn(\mathbf{Lk})_3]^{2+}$ is larger than that produced by the up−up−down organization of three unsymmetrical ligands in the C_1-symmetrical *mer*-$[Zn(\mathbf{Lk})_3]^{2+}$ isomer,[16d,43] we tentatively assign the enthalpic stabilization of the facial complex to a simple dielectric effect.[44] Taking solvation effects as the predominant factor controlling eq 18, one predicts that the complex with the largest electric dipole moment, namely, *fac*-$[Zn(\mathbf{Lk})_3]^{2+}$, provides the largest contribution to the organization of the polar solvent molecules.[45] This translates into an additional negative entropic contribution to eq 18, which shifts $\Delta S^{Zn,Lk}_{mer\rightarrow fac}$ below its statistical value of −9.1 J/mol·K (Table 4).

Isolation and Crystal Structures of the Complexes $[Zn(Lk)_n](CF_3SO_3)_2$ (Lk = L1, L3; *n* = 2−3). Diffusion of diethyl ether into concentrated acetonitrile solutions containing either **L1** or **L3** (3 equiv) with $Zn(CF_3SO_3)_2$ (1 equiv) gave 92−93% yields of microcrystalline powders whose elemental analyses correspond to $[Zn(\mathbf{L1})_3](CF_3SO_3)_2$ and $[Zn(\mathbf{L3})_3](CF_3SO_3)_2$. Recrystallization from nitromethane/diethyl ether provided X-ray quality prisms of $[Zn(\mathbf{L1})_3](CF_3SO_3)_2(H_2O)_{0.5}$ and $[Zn(\mathbf{L3})_3](CF_2SO_3)_2$ (Figures S24−S26 and Tables S7−S11 in the Supporting Information). In line with the predominance of the meridional isomers in solution at room temperature (Figure 5), the crystal structures of the complexes isolated in the solid state show distorted pseudo-octahedral $[Zn(\mathbf{L1})_3]^{2+}$ and $[Zn(\mathbf{L3})_3]^{2+}$ cations adopting the meridional conformation, together with noncoordinated anionic triflates and solvent molecules (Figure 6). Three categories of Zn−N distances are observed. The stronger interactions are found for

dx.doi.org/10.1021/ic5022559 | Inorg. Chem. 2014, 53, 13093−13104

the connection of the benzimidazole rings with the central zinc atom ($Zn-N_{bzim}$ = 2.11(2) Å in $[Zn(\mathbf{L1})_3]^{2+}$ and 2.09(7) Å in $[Zn(\mathbf{L3})_3]^{2+}$), followed by the coordination of the pyridine rings ($Zn-N_{pyridine}$ = 2.24(4) Å in $[Zn(\mathbf{L1})_3]^{2+}$) and of the pyrazine rings ($Zn-N_{pyrazine}$ = 2.27(3) Å in $[Zn(\mathbf{L3})_3]^{2+}$). This trend correlates with the decreasing proton affinities measured in water (pK_a(bzim) = 5.68 > pK_a(pyridine) = 5.23 > pK_a(pyrazine) = 0.65).[37] We however cannot detect any sign of structural trans influence,[23] the $Zn-N_{bzim}$ distances being statistically distributed around their average values, whatsoever the nature of the nitrogen atom bound trans to the benzimidazole ring. The interchelate angles found for $[Zn(\mathbf{L1})_3]^{2+}$ (average value: 87.1(7)°) and $[Zn(\mathbf{L3})_3]^{2+}$ (average value: 84.3(2.4)°) are close to those predicted for a perfect octahedron (90°), and the only noticeable difference concerns the interplanar angle α between the two aromatic rings within each didentate ligand, which is larger for the pyrazine–benzimidazole units in $[Zn(\mathbf{L3})_3]^{2+}$ (α = 21(13)°) than it is in $[Zn(\mathbf{L1})_3]^{2+}$ (α = 12(9)°, see Figure S26 in the Supporting Information).

Attempts to isolate $[Zn(\mathbf{Lk})]^{2+}$ (1:1 stoichiometry) complexes only failed, but slow diffusion of diethyl ether into concentrated acetonitrile solutions containing **Lk** (1 equiv) and $Zn(CF_3SO_3)_2$ (1 equiv) gave small amounts of X-ray quality prisms of $[Zn(\mathbf{L1})_2(CF_3SO_3)(OH_2)](CF_3SO_3)(CH_3CN)$ and $[Zn(\mathbf{L3})_2(CF_3SO_3)_2](CH_3CN)$ (1:2 stoichiometries; Figure S27 and Tables S12–S16 in the Supporting Information). The molecular structures of $[Zn(\mathbf{L1})_2(CF_3SO_3)(OH_2)]^+$ and $[Zn(\mathbf{L3})_2(CF_3SO_3)_2]$ are globally superimposable (Supporting Information, Figure S28) and correspond to cis–fac isomers (Figure 7, the terminology is explained in Scheme 3). Again, no significant trans influence can be highlighted from the analysis of interatomic bond lengths within experimental errors.

CONCLUSION

In terms of free energy, the thermodynamic trans influence operating in $[Zn(\alpha,\alpha'\text{-diimine})_3]^{2+}$ complexes corresponds to a minor contribution to the complexation process, which favors *fac*-$[Zn(\mathbf{Lk})_3]^{2+}$ (three N_A-Zn-N_B trans correlations) over *mer*-$[Zn(\mathbf{Lk})_3]^{2+}$ (one N_A-Zn-N_B trans correlation) at low temperature ($0 \le \Delta E^{\mathbf{Lk},\mathbf{Lk}}_{cis,mer} - \Delta E^{\mathbf{Lk},\mathbf{Lk}}_{cis,fac} \le 2$ kJ·mol^{-1} at 233 K). We also note that the trans influence is slightly improved when the pyridine ring in **L1** and **L2** is replaced with the less donating pyrazine ring in **L3** and **L4**. Since (i) the meridional → facial isomerization process is driven by enthalpy but offset at room temperature by an opposite entropic contribution and (ii) the trans influence could not be detected in the solid state, we conclude that the trans influence occurring in pseudo-octahedral $[Zn(\alpha,\alpha'\text{-diimine})_3]^{2+}$ complexes originates from intermolecular solvation effects. This behavior contrasts with the related mer → fac isomerization processes operating in pseudotricapped trigonal prismatic $[Ln(2,6\text{-bis(benzimidazol-2'-yl)pyridine})_3]^{3+}$ complexes, which are controlled by intramolecular interstrand packing interactions occurring between the bound ligand strands (Ln is a spherical trivalent lanthanide).[36c] The selective and quantitative (>95%) formation of the *fac*-$[Zn(\mathbf{Lk})_3]^{2+}$ isomers (**L1**–**L3**) thus requires the combination of the trans influence with some additional thermodynamic driving force, brought, for instance, by the use of a noncovalent lanthanide tripod in the self-assembled $[EuZn(\mathbf{L6})_3]^{5+}$[22a] and $[EuZn(\mathbf{L7})_3]^{5+}$ complexes (Figure 8a,b and Supporting Information, Figure S29, Tables S17–S19, and Appendix 3).

Application of the site binding model to the *mer*-$[EuZn(\mathbf{Lk})_3]^{5+}$ → *fac*-$[EuZn(\mathbf{Lk})_3]^{5+}$ isomerization shows that the exchange constants $K^{Zn,Eu,\mathbf{Lk}}_{mer\rightarrow fac}$ primarily include the unfavorable 0.2–0.7 factor ($(1/3)\cdot((u^{\mathbf{Lk},\mathbf{Lk}}_{cis,fac})/(u^{\mathbf{Lk},\mathbf{Lk}}_{cis,mer}))^2$ in Figure 8c), which stands for the unfavorable meridional-to-facial isomerization processes occurring around Zn(II) ($K^{Zn,\mathbf{Lk}}_{mer\rightarrow fac}$ in eq 20 and in Table 4). However, the target facial isomers *fac*-$[EuZn(\mathbf{Lk})_3]^{5+}$ benefit from the intramolecular binding of one supplementary terminal N_2O tridentate binding site to the remote Eu(III) cation ($f^{Eu,N_2O}\cdot EM\cdot(u^{\mathbf{Lk},\mathbf{Lk}}_{tri,tri})^2$ in Figure 8c, EM is the effective molarity). Introducing the experimental values for the affinity of the europium for the tridentate binding unit ($f^{Eu,N_2O} = 10^{5.5}$), for the effective molarity controlling the intramolecular macrocyclization reaction ($EM = 10^{-3.9}$) and for the intramolecular interligand interaction between two tridentate binding units bound to europium cation ($u^{\mathbf{Lk},\mathbf{Lk}}_{tri,tri} = 10^{-0.1}$) in acetonitrile,[41] we estimate $f^{Eu,N_2O}\cdot EM\cdot(u^{\mathbf{Lk},\mathbf{Lk}}_{tri,tri})^2 \approx 40$. The latter contribution overcomes by 1 order of magnitude the unfavorable $K^{Zn,\mathbf{Lk}}_{mer\rightarrow fac}$ exchange constant, thus leading to the exclusive formation of the C_3-symmetrical *fac*-$[EuZn(\mathbf{Lk})_3]^{5+}$ isomer in the solid state (Figure 8b) and in solution at millimolar concentrations (Supporting Information, Figure S30).

ASSOCIATED CONTENT

Supporting Information

Details for the activation of 5-methyl-2-pyrazinecarboxylic acid (Appendix 1) and for the synthesis of ligand L7 (Appendix 3). Determination of statistical factors for chemical reactions (Appendix 2). Tables of crystal data (Tables S1–S5 and S7–S19) and thermodynamic data (Table S6). Figures showing molecular structures (Figures S1, S24–S29, and S30), ^{1}H NMR data (Figures S2, S8–S11, and S20–S23), spectrophotometric data (Figures S3–S6), and thermodynamic data (Figures S7 and S12–S19). The CIF files for **L1**, **L3**, **L5** $[Zn(\mathbf{L1})_3](CF_3SO_3)_2(H_2O)_{0.5}$, $[Zn(\mathbf{L3})_3](CF_2SO_3)_2$ $[Zn(\mathbf{L1})_2(CF_3SO_3)(OH_2)](CF_3SO_3)(CH_3CN)$, $[Zn(\mathbf{L3})_2(CF_3SO_3)_2](CH_3CN)$, and $[EuZn(\mathbf{L7})_3](CF_3SO_3)_5(H_2O)_3(CH_3OH)(CH_3CN)_{0.5}$. This material is available free of charge via the Internet at http://pubs.acs.org. CCDC 1022919–1022926 contain the supplementary crystallographic data. The cif files can be obtained free of charge via www.ccdc.cam.ac.uk/conts/retrieving.html (or from the Cambridge Crystallographic Data Centre, 12 Union Road, Cambridge CB2 1EZ, U.K.; fax: (+ 44) 1223–336–033; or deposit@ccdc.cam.ac.uk).

AUTHOR INFORMATION

Corresponding Author

*E-mail: Claude.Piguet@unige.ch.

Author Contributions

§These authors contributed equally to this research work.

Notes

The authors declare no competing financial interest.

ACKNOWLEDGMENTS

We thank Prof. Y. Filinchuk and the Swiss Norwegian Beamlines (ESRF, Grenoble, France) for single-crystal X-ray diffraction measurement. Financial support from the Swiss National Science Foundation is gratefully acknowledged.

REFERENCES

(1) (a) Purcell, K. F.; Kotz, J. C. *Inorganic Chemistry;* W.B. Saunders Company: Hong Kong, 1978. (b) Cotton, F. A.; Wilkinson, G. *Advanced Inorganic Chemistry,* 4th ed.; John Wiley & Sons: New York, 1980. (c) Greenwood, N. N.; Earnshaw, A. *Chemistry of the Elements,* 2nd ed.; Butterworth and Heinemann: Oxford, U.K., 1997. (d) Housecroft, C. E.; Constable, E. C. *Chemistry,* 4th ed.; Pearson Education Limited: Upper Saddle River, NJ, 2010.

(2) (a) Schwarzenbach, G. *Helv. Chim. Acta* **1952**, *35*, 39−65. (b) Martell, A. E. *Adv. Chem. Ser.* **1966**, *62*, 272−294.

(3) (a) Koenig, E. *Coord. Chem. Rev.* **1968**, *3*, 471−495. (b) McWhinnie, W. R.; Miller, J. D. *Adv. Inorg. Chem. Radiochem.* **1969**, *12*, 135−215. (c) Gillard, R. D. *Coord. Chem. Rev.* **1975**, *16*, 67−94. (d) Constable, E. C. *Adv. Inorg. Chem.* **1989**, *34*, 1−63. (e) Hamacek, J.; Borkovec, M.; Piguet, C. *Dalton Trans.* **2006**, 1473−1490. (f) Happ, B.; Winter, A.; Hager, M. D.; Schubert, U. S. *Chem. Soc. Rev.* **2012**, *41*, 2222−2255.

(4) For reviews, see (a) Meyer, T. J. *Pure Appl. Chem.* **1986**, *58*, 1193−1206. (b) Polo, A. S.; Itokazu, M. K.; Murakami, I.; Neyde, Y. *Coord. Chem. Rev.* **2004**, *248*, 1343−1361. (c) Balzani, V.; Bergamini, G.; Marchioni, F.; Ceroni, P. *Coord. Chem. Rev.* **2006**, *250*, 1254−1266. (d) Concepcion, J. J.; Jurss, J. W.; Brennaman, M. K.; Hoertz, P. G.; Patrocinio, A.; Otavio, T.; Murakami, I.; Neyde, Y.; Templeton, J. L.; Meyer, T. J. *Acc. Chem. Res.* **2009**, *42*, 1954−1965. (e) Wagenknecht, P. S.; Ford, P. C. *Coord. Chem. Rev.* **2011**, *255*, 591−616. (f) Happ, B.; Winter, A.; Hager, M. D.; Schubert, U. S. *Chem. Soc. Rev.* **2012**, *41*, 2222−2255. (g) Thompson, D. W.; Ito, A.; Meyer, T. J. *Pure Appl. Chem.* **2013**, *85*, 1257−1305.

(5) (a) Balzani, V.; Juris, A.; Venturi, M.; Campagna, S.; Serroni, S. *Chem. Rev.* **1996**, *96*, 759−833. (b) Fletcher, N. C.; Keene, F. R.; Vierborock, H.; von Zelewsky, A. *Inorg. Chem.* **1997**, *36*, 1113−1121. (c) Keene, F. R. *Chem. Soc. Rev.* **1998**, *27*, 185−193. (d) Knopf, U.; von Zelewsky, A. *Angew. Chem., Int. Ed. Engl.* **1999**, *38*, 302−322. (e) MacDonnel, F. M.; Kim, M. J.; Bodige, S. *Coord. Chem. Rev.* **1999**, *186*, 535−549. (f) Newkome, G. R.; Patri, A. K.; Holder, E.; Schubert, U. S. *Eur. J. Org. Chem.* **2004**, *2*, 235−254. (g) Hapke, M.; Brandt, L.; Luetzen, A. *Chem. Soc. Rev.* **2008**, *37*, 2782−2797. (h) Fan, J.; Autschbach, J.; Ziegler, T. *Inorg. Chem.* **2010**, *49*, 1355−1362. (i) Lacour, J.; Hebbe-Viton, V. *Chem. Soc. Rev.* **2003**, *32*, 373−382. (j) Keene, F. R. *Dalton Trans.* **2011**, *40*, 2405−2418.

(6) (a) Singh, K.; Long, J. R.; Stavropoulos, P. *Inorg. Chem.* **1998**, *37*, 1073−1079. (b) Halcrow, M. A. *Polyhedron* **2007**, *26*, 3523−3576. (c) Najar, A. M.; Tidmarsh, I. S.; Ward, M. D. *Inorg. Chem.* **2009**, *48*, 11871−11881. (d) Halcrow, M. A. *Dalton Trans.* **2009**, 2059−2073.

(7) Holm, R. H. In *Dynamic Nuclear Magnetic Resonance Spectroscopy;* Jackman, L. M., Cotton, F. A., Eds.; Academic Press: New York, 1975.

(8) Ercolani, G.; Piguet, C.; Borkovec, M.; Hamacek, J. *J. Phys. Chem. B* **2007**, *111*, 12195−12203.

(9) (a) Sloan, T. E. *Top. Stereochem.* **1981**, *12*, 1−36. (b) Jarjayes, O.; Hamman, S.; Brochier, M.-C.; Béguin, C.; Nardin, R. *Magn. Reson. Chem.* **2000**, *38*, 360−365.

(10) Furushou, D.; Hashibe, T.; Fujinami, T.; Nishi, K.; Hagiwara, H.; Matsumoto, N.; Sunatsuki, Y.; Kojima, M.; Iijima, S. *Polyhedron* **2013**, *52*, 1489−1498.

(11) (a) Tamayo, A. B.; Alleyne, B. D.; Djurovich, P. I.; Lamansky, S.; Tsyba, I.; Ho, N. H.; Bau, R.; Thompson, M. E. *J. Am. Chem. Soc.* **2003**, *125*, 7377−7387. (b) Wang, J.; Oyler, K. D.; Bernhard, S. *Inorg. Chem.* **2007**, *46*, 5700−5706.

(12) (a) Rutherford, T. J.; Keene, F. R. *J. Chem. Soc., Dalton Trans.* **1998**, 1155−1162. (b) Yeomans, B. D.; Kelso, L. S.; Tregloan, P. A.; Keene, F. R. *Eur. J. Inorg. Chem.* **2001**, 239−246.

(13) (a) Cheng, L. F.; Lia, L. S.; Lai, W. Y.; Sun, X. H.; Wong, N. B.; Lee, C. S.; Lee, S. T. *Chem. Phys. Lett.* **2000**, *319*, 418−422. (b) Qin, D. S.; Li, D. C.; Wang, Y.; Zhang, J. D.; Xie, Z. Y.; Wang, G.; Wang, L. X. *Appl. Phys. Lett.* **2001**, *78*, 437−439.

(14) (a) Curioni, A.; Boero, M.; Andreoni, W. *Chem. Phys. Lett.* **1998**, *294*, 263−271. (b) Katakura, R.; Koide, Y. *Inorg. Chem.* **2006**, *45*, 5730−5732.

(15) Charbonnière, L. J.; Williams, A. F.; Frey, U.; Merbach, A. E.; Kamalaprija, P.; Schaad, O. *J. Am. Chem. Soc.* **1997**, *119*, 2488−2496.

(16) (a) Gromova, M.; Jarjayes, O.; Hamman, S.; Nardin, R.; Béguin, C.; Willem, R. *Eur. J. Inorg. Chem.* **2000**, 545−550. (b) Utz, M.; Chen, C.; Morton, M.; Papadimitrakopoulos, F. *J. Am. Chem. Soc.* **2003**, *125*, 1371−1375. (c) Ramos, M. L.; de Sousa, A. R. E.; Justino, L. L. G.; Fonseca, S. M.; Geraldes, C. F. G. C.; Burrows, H. D. *Dalton Trans.* **2013**, *42*, 3682−3694. (d) Iwakura, I.; Ebina, H.; Komori-Orisaku, K.; Koide, Y. *Dalton Trans.* **2014**, *43*, 12824−12827.

(17) (a) Fletcher, N. C.; Nieuwenhuyzen, M.; Rainey, S. *J. Chem. Soc., Dalton Trans.* **2001**, 2641−2648. (b) Grabulosa, A.; Beley, M.; Gros, P. C. *Eur. J. Inorg. Chem.* **2008**, 1747−1751.

(18) (a) Torelli, S.; Delahaye, S.; Hauser, A.; Bernardinelli, G.; Piguet, C. *Chem.—Eur. J.* **2004**, *10*, 3503−3516. (b) Riis-Johannessen, T.; Dupont, N.; Canard, G.; Bernardinelli, G.; Hauser, A.; Piguet, C. *Dalton Trans.* **2008**, 3661−3677.

(19) Since three microspecies contribute to the meridional isomer and only one exists for the facial isomer, the pure entropic contribution to the free energy change is given by $\Delta G^{\circ,\mathrm{mer}\rightarrow\mathrm{fac}}_{\mathrm{exch,stat}} = -RT\ln(K^{\mathrm{mer}\rightarrow\mathrm{fac}}_{\mathrm{exch,stat}})$, $= -T\Delta S^{\mathrm{mer}\rightarrow\mathrm{fac}}_{\mathrm{exch,stat}} = -RT\ln(1/3) = 2.7\ \mathrm{kJ} \times \mathrm{mol}^{-1}$.

(20) (a) Appleton, T. J.; Clark, H. C.; Manzer, L. E. *Coord. Chem. Rev.* **1973**, *10*, 335−422. (b) Coe, B. J.; Glenwright, S. J. *Coord. Chem. Rev.* **2000**, *203*, 5−80.

(21) (a) Josceanu, A. M.; Moore, P. *J. Chem. Soc., Dalton Trans.* **1998**, 369−374. (b) Weizman, H.; Libman, J.; Shanzer, A. *J. Am. Chem. Soc.* **1998**, *120*, 2188−2189. (c) Fletcher, N. C.; Martin, C.; Abraham, H. J. *New J. Chem.* **2007**, *31*, 1407−1411. (d) Seredyuk, M.; Munoz, M. C.; Ksenofontov, V.; Gütlich, P.; Galyametdinov, Y.; Real, J. A. *Inorg. Chem.* **2014**, *53*, 8442−8454.

(22) (a) Piguet, C.; Bünzli, J.-C. G.; Bernardinelli, G.; Hopfgartner, G.; Petoud, S.; Schaad, O. *J. Am. Chem. Soc.* **1996**, *118*, 6681−6697. (b) Piguet, C.; Rivara-Minten, E.; Bernardinelli, G.; Bünzli, J.-C. G.; Hopfgartner, G. *J. Chem. Soc., Dalton Trans.* **1997**, 421−433. (c) Cantuel, M.; Bernardinelli, G.; Imbert, D.; Bünzli, J.-C. G.; Hopfgartner, G.; Piguet, C. *J. Chem. Soc., Dalton Trans.* **2002**, 1929−1940.

(23) Anderson, K. M.; Orpen, A. G. *Chem. Commun.* **2001**, 2682−2683.

(24) (a) Gampp, H.; Maeder, M.; Meyer, C. J.; Zuberbühler, A. *Talanta* **1985**, *32*, 1133−1139. (b) Maeder, M.; King, P. Analysis of Chemical Processes, Determination of the Reaction Mechanism and Fitting of Equilibrium and Rate Constants. In *Chemometrics in Practical Applications,* Varmuza, K., Dr., Ed.; ISBN: 9789535104384, DOI: 10.5772/31896. (c) Specfit/32 from ReactLab Equilibria: http://jplusconsulting.com/products/reactlab-equilibria/.

(25) (a) Sheldrick, G. M.SHELXS97. In *Acta Crystallogr., Sect. A,* **2008**, *64*, 112−122. (b) SIR97. Altomare, A.; Burla, M. C.; Camalli, M.; Cascarano, G. L.; Giacovazzo, C.; Guagliardi, A.; Moliterni, A. G. G.; Polidori, G.; Spagna, R. *J. Appl. Crystallogr.* **1999**, *32*, 115−119. (c) SIR92 Altomare, A.; Cascarano, G.; Giacovazzo, C.; Guagliardi, A. *J. Appl. Crystallogr.* **1993**, *26*, 343−350.

(26) Sheldrick, G. M. *Acta Crystallogr., Sect. A* **2008**, *64*, 112−122.

(27) Betteridge, P. W.; Carruthers, J. R.; Cooper, R. I.; Prout, K.; Watkin, D. J. *J. Appl. Crystallogr.* **2003**, *36*, 1487.

(28) Piguet, C.; Bocquet, B.; Hopfgartner, G. *Helv. Chim. Acta* **1994**, *77*, 931−942.

(29) (a) Ambrogi, V.; Cozzi, P.; Sanjust, P.; Bertone, L.; Lavisolo, P.; Bratico Vangosa, G.; Angelucci, R. *Eur. J. Med. Chem.* **1980**, *15*, 157−163. (b) Eiichi, M.; Iwasaki, N.; Yagi, N.; Ohashi, T.; Kato, H.; Ito, Y.; Azuma, H. *Chem. Pharm. Bull.* **1990**, *65*, 201−207.

(30) McKenzie, B. M.; Miller, A. K.; Wojtecki, R. J.; Johnson, J. C.; Burke, K. A.; Tzeng, K. A.; Mather, P. T.; Rowan, S. J. *Tetrahedron* **2008**, *64*, 8488−8495.

(31) Cukrowski, I.; de Lange, J. H.; Mitoraj, M. *J. Phys. Chem. A* **2014**, *118*, 623−637.

(32) Hoang, T. N.; Lathion, T.; Guénée, L.; Terazzi, E.; Piguet, C. *Inorg. Chem.* **2012**, *51*, 8567−8575.

(33) (a) Malinowski, E. R.; Howery, D. G. *Factor Analysis in Chemistry;* Wiley: New York, Chichester, 1980. (b) Gampp, H.;

Maeder, M.; Meyer, C. J.; Zuberbühler, A. *Talanta* **1986**, *33*, 943−951. (c) Hall, B. R.; Manck, L. E.; Tidmarsh, I. S.; Stephenson, A.; Taylor, B. F.; Blaikie, E. J.; Vander Griend, D. A.; Ward, M. D. *Dalton Trans.* **2011**, *40*, 12132−12145.
(34) Riis-Johannessen, T.; Bernardinelli, G.; Filinchuk, Y.; Clifford, S.; Dalla Favera, N.; Piguet, C. *Inorg. Chem.* **2009**, *48*, 5512−5525.
(35) Charbonnière, L. J.; Williams, A. F.; Piguet, C.; Bernardinelli, G.; Rivara-Minten, E. *Chem.—Eur. J.* **1998**, *4*, 485−493.
(36) (a) Piguet, C.; Bünzli, J.-C. G.; Bernardinelli, G.; Williams, A. F. *Inorg. Chem.* **1993**, *32*, 4139−4149. (b) Piguet, C.; Bünzli, J.-C. G.; Bernardinelli, G.; Bochet, C. G.; Froidevaux, P. J. *Chem. Soc., Dalton Trans.* **1995**, 83−97. (c) Le Borgne, T.; Altmann, P.; André, N.; Bünzli, J.-C. G.; Bernardinelli, G.; Morgantini, P.-Y.; Weber, J.; Piguet, C. *Dalton Trans.* **2004**, 723−733.
(37) CRC Handbook of Chemistry and Physics, Internet version 2005, Lide, D. R., Ed.; http://www.hbcpnetbase.com; CRC Press: Boca Raton, FL, 2005.
(38) (a) Borkovec, M.; Hamacek, J.; Piguet, C. *Dalton Trans.* **2004**, 4096−4105. (b) Piguet, C. *Chem. Commun.* **2010**, *46*, 6209−6231.
(39) Benson, S. W. *J. Am. Chem. Soc.* **1958**, *80*, 5151−5154.
(40) Willcott, M. R.; Lenkinski, R. E.; Davis, R. E. *J. Am. Chem. Soc.* **1972**, *94*, 1742−1744.
(41) Riis-Johannessen, T.; Dalla Favera, N.; Todorova, T. K.; Huber, S. M.; Gagliardi, L.; Piguet, C. *Chem.—Eur. J.* **2009**, *15*, 12702−12718.
(42) During the global fitting process, four parameters are fitted to five equations. Please note that eqs 13−15 and 19 are mathematically independent, while eq. 18 is correlated, but its independent determination by NMR is used as an additional constraint to the system. We did not correct the stability constants for the change in temperature. Formation constants are obtained at 298 K and exchange constants at 233 K.
(43) The Neumann's principle implies that one direction of the general quadric must be aligned with the axis of highest symmetry. (a) Nye, J. F. *Physical Properties of Crystals;* Clarendon Press: Oxford, U.K., 1985. (b) Haussühl, S. *Kristallphysik;* Physic-Verlag: Weinheim, Germany, 1983.
(44) (a) Onsager, L. *J. Am. Chem. Soc.* **1936**, *58*, 1486−1492. (b) Matyushov, D. V. *J. Chem. Phys.* **2004**, *120*, 1375−1382. (c) Cramer, C. J.; Truhlar, D. G. *Acc. Chem. Res.* **2008**, *41*, 760−768.
(45) Motekaitis, R. J.; Martell, A. E.; Hancock, R. D. *Coord. Chem. Rev.* **1994**, *133*, 39−65.